Investigation of the Critical Currents in Thin-Film MoGe Devices

Ivan P. Nevirkovets, Scott T. Grudichak, Mikhail Belogolovskii, and John B. Ketterson

***Abstract*—We report on flux-flow properties of 50 nm thick thin-film amorphous MoGe bridges of different sizes with and without patterned sub-micron holes with different diameters and spacings. Characterization of the devices was carried out in liquid He at 4.2 K in a magnetic field, H, applied perpendicular to the device plane. Two critical currents, I_{c1} and I_{c2}, were studied. The current I_{c1} is identified as the onset of a low-resistance state, whereas I_{c2} is the current at which the device switches to a high-resistance state, and the corresponding dependences $I_{c1}(H)$ and $I_{c2}(H)$ were determined. In the absence of the holes, I_{c1} decreases monotonically with H, whereas $I_{c2}(H)$ manifests lobes resembling those in the Fraunhofer-like pattern characteristic of Josephson junctions. This behavior may be due to formation of an ordered vortex lattice in some current and field ranges. Introducing the hole-line arrays modifies both $I_{c1}(H)$ and $I_{c2}(H)$ in a way that is most complicated for larger hole diameters.**

***Index Terms*—Flux flow, hole arrays, magnetic vortices, superconducting microbridges, superconductivity, thin films.**

I. Introduction

STUDYING nucleation of Abrikosov vortices and their influence on the superconducting state in thin films is important from both fundamental and practical points of view (see, e. g., reviews [1], [2], [3]). When the vortex flow takes place, the superconductor enters a resistive state, which leads to power dissipation. In order to support the superconducting state when the electric current and an external magnetic field are applied, one needs to immobilize vortex movement by pinning them on defects. A convenient way to study the vortex pinning is to introduce artificial defects, for example, holes. In this work, we study both static and dynamic pinning in unpatterned microbridges and in several types of hole arrays made in 50-nm thick MoGe film.

Manuscript received 22 September 2023; revised 3 December 2023; accepted 12 December 2023. Date of publication 20 December 2023; date of current version 28 December 2023. The work of Mikhail Belogolovskii was supported by EU NextGenerationEU through the Recovery and Resilience Plan for Slovakia under Project 09I03-03-V01-00139. This work was supported in part by NSF under Grant DMR 1905742 and in part by the NSF DISCoVER Expedition under Grant CCF- 2124453. *(Corresponding author: Ivan P. Nevirkovets.)*

Ivan P. Nevirkovets and Scott T. Grudichak are with the Department of Physics and Astronomy, Northwestern University, Evanston, IL 60208 USA (e-mail: inevirkovets@northwestern.edu; scottgrudichak2021@u.northwestern.edu).

Mikhail Belogolovskii is with the Department of Experimental Physics, Faculty of Mathematics, Physics and Informatics, Comenius University Bratislava, 84248 Bratislava, Slovakia (e-mail: belogolovskii@ukr.net).

John B. Ketterson is with the Department of Physics and Astronomy and the Department of Electrical and Computer Engineering, Northwestern University, Evanston, IL 60208 USA (e-mail: j-ketterson@northwestern.edu).

Color versions of one or more figures in this article are available at https://doi.org/10.1109/TASC.2023.3343324.

Digital Object Identifier 10.1109/TASC.2023.3343324

There are several reasons to use the amorphous superconductor $Mo_{1-x}Ge_x$ (with the critical temperature T_c up to about 7 K) for vortex flow studies. First, thin films of this material have proven to be of high quality, with a smooth surface, and without discontinuities, even at very small thicknesses [4]. As a result of high uniformity and absence of defects, vortex pinning in amorphous films is very low, which, in turn, allows one to study free flux-flow and self-organized vortex lattices in both the static and dynamic states [5], [6]. Finally, it appears that, unlike Nb films, the *I–V* curve of a MoGe microbridge has an extended region of flux flow in an applied magnetic field, which enables studying a wide range of vortex lattice drift velocities.

II. Experimental

Here we report on flux-flow properties of 50 nm thick amorphous MoGe bridges of different sizes, with and without patterned sub-micron holes with different diameters and spacings formed by focused ion beam (FIB). The $Mo_{1-x}Ge_x$ films were deposited onto oxidized Si substrates by magnetron sputtering from a $Mo_{75}Ge_{25}$ target at room temperature. Microbridges of different sizes were patterned using optical lithography and reactive ion etching (RIE) in SF_6 plasma. Characterization of the devices was carried out in liquid He at 4.2 K in a magnetic field, H, applied perpendicular to the device plane. Magnetic field was produced by a superconducting solenoid allowed for application of maximum field of about 600 Oe at 4.2 K. Two critical currents, I_{c1} and I_{c2}, were studied. Critical current I_{c1} is defined as the current for the onset of the resistive branch in the *I–V* curve, whereas I_{c2} is the maximum current of the branch, above which the flux flow instability occurs driving the sample into a high-resistance state (see Fig. 1).

III. Results and Discussion

Fig. 2 shows the $I_{c1}(H)$ (solid symbols) and $I_{c2}(H)$ (open symbols) dependences for unpatterned samples with $L = 10$ μm (royal and magenta symbols) and $L = 15$ μm (blue and red symbols) and $w = 10$ μm. Voltage criteria for detecting I_{c1} were from 5 μV to 15 μV in different samples, dependent on the noise level. Voltage criterion for I_{c2} was set to be slightly larger than the maximum voltage of the initial resistive branch in the *I–V* curve. The modulation patterns shown here are for an external magnetic field (applied perpendicular to the sample plane) swept in two opposite directions; therefore, each $I_c(H)$ pattern contains two curves.

1051-8223 © 2023 IEEE. Personal use is permitted, but republication/redistribution requires IEEE permission.
See https://www.ieee.org/publications/rights/index.html for more information.

Authorized licensed use limited to: Northwestern University. Downloaded on February 18,2024 at 00:22:00 UTC from IEEE Xplore. Restrictions apply.

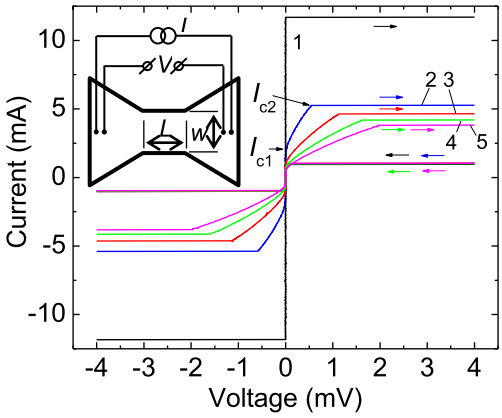

Fig. 1. Family of *I*–*V* curves of an unpatterned microbridge with $L = w = 10$ μm taken for different magnetic fields at 4.2 K. Curves from 1 to 5 are for $H = 0$, 111, 222, 333, and 444 Oe, respectively. Inset shows a schematic of the sample and its biasing (top view).

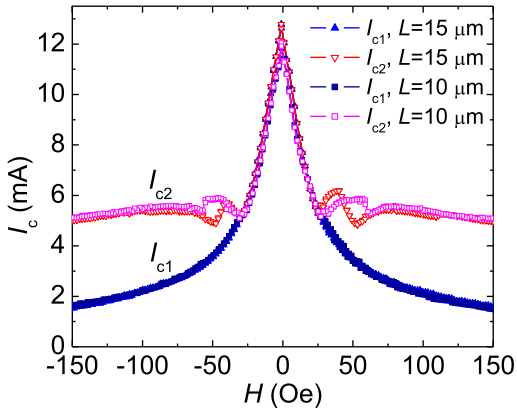

Fig. 2. $I_{c1}(H)$ (solid symbols) and $I_{c2}(H)$ (open symbols) dependences for the samples with $L = 15$ μm (blue and red symbols) and $L = 10$ μm (royal and magenta symbols) and $w = 10$ μm.

A peculiar feature of the $I_{c2}(H)$ dependence is its nonmonotonic dependence, unlike the $I_{c1}(H)$ dependence that displays monotonic decay of I_{c1} with H. Specifically, there are additional side maxima whose width depends on the sample size; this resembles the $I_c(H)$ dependence of a Josephson junction. A possible explanation of this effect is that, due to a very weak vortex pinning in MoGe films, a coherent motion of the vortices forming a regular lattice is possible in some current and field ranges. The Pearl length in thin films, which determines the extent of electromagnetic fields and currents around the vortex core, is $\Lambda = 2\lambda^2/d$, where λ is the London depth, and d is the film thickness [7]. Using $\lambda(4.2\ \mathrm{K}) = 500$ nm in our MoGe films [8], and $d = 50$ nm, we obtain $\Lambda = 10$ μm. Therefore, the Pearl length at 4.2 K is on the order of the microbridge size, meaning that the long-range interaction between the vortices extends over the entire microbridge area, favoring their coherent motion. The minimum in the $I_{c2}(H)$ dependence may occur when the vortex line enters the side of the bridge. Not so pronounced as in our case, a feature in the dependence of instability current on an applied magnetic field for a Mo_3Ge microbridge was reported by Grimaldi et al. [9].

Introducing a hole-line array running across the bridge (i.e., perpendicular to the current flow) modifies both $I_{c1}(H)$ and $I_{c2}(H)$ in a way that is most complicated for larger hole diameters.

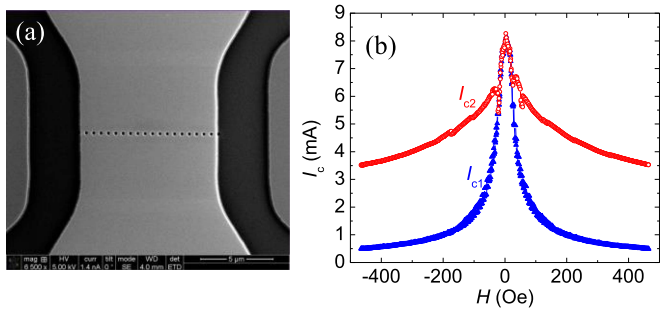

Fig. 3. (a) SEM image of the hole-line array with the following parameters: MoGe film thickness: 50 nm; microbridge dimensions: 10 μm × 10 μm; nominal hole diameter: 150 nm; nominal spacing: 500 nm. (b) $I_{c1}(H)$ (blue triangles) and $I_{c2}(H)$ (red open circles) dependences.

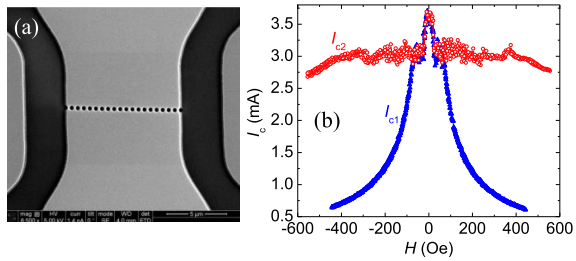

Fig. 4. (a) SEM image of the hole-line array with the following parameters: MoGe film thickness: 50 nm; microbridge dimensions: 10 μm × 10 μm; nominal hole diameter: 300 nm; nominal spacing: 500 nm. (b) $I_{c1}(H)$ (blue triangles) and $I_{c2}(H)$ (red open circles) dependences.

In comparison with the unpatterned microbridges, line arrays introduce distortion of the $I_{c2}(H)$ pattern, but $I_{c1}(H)$ experiences little change until the diameter of the holes becomes large, and the spacing between them becomes small. Fig. 3(a) shows an SEM image of the line array made in 50 nm thick MoGe microbridge with lateral dimensions of 10 μm × 10 μm. Nominal hole diameter is 150 nm; nominal spacing between the holes is 500 nm. Fig. 3(b) shows $I_{c1}(H)$ (solid blue triangles) and $I_{c2}(H)$ (open red circles) dependences. The $I_{c2}(H)$ pattern displays asymmetry and additional side maxima compared with the $I_{c2}(H)$ dependence for unpatterned sample.

Fig. 4(a) shows an SEM image of the hole-line array with nominal hole diameter of 300 nm; nominal spacing between the holes is 500 nm. The array is made in a 50 nm thick MoGe microbridge with lateral dimensions of 10 μm × 10 μm. Fig. 4(b) shows $I_{c1}(H)$ (solid blue triangles) and $I_{c2}(H)$ (open red circles) dependences. In this case, $I_{c1}(H)$ is likely determined by parallel array of Josephson-type nanobridges, whereas noisy $I_{c2}(H)$ dependence is likely due to flux noise usually observed in SQUIDs.

We also fabricated and studied characteristics of a hole-line array wherein the line is oriented parallel to current flow (in-line array); see an SEM image of the array in Fig. 5(a). The array is made in a 50 nm thick MoGe microbridge with lateral dimensions of 10 μm × 10 μm. The nominal hole diameter is 200 nm; the nominal lattice period is 400 nm. Fig. 5(b) shows $I_{c1}(H)$ (solid blue triangles) and $I_{c2}(H)$ (open red circles) dependences. The shape of the $I_{c1}(H)$ pattern is similar to that

Authorized licensed use limited to: Northwestern University. Downloaded on February 18,2024 at 00:22:00 UTC from IEEE Xplore. Restrictions apply.

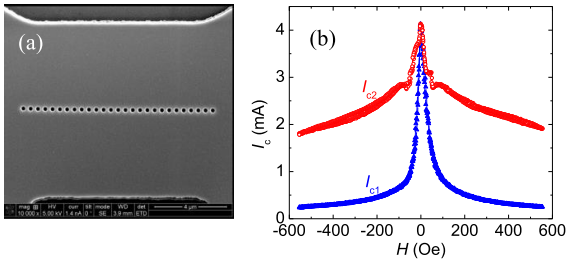

Fig. 5. (a) SEM image of the in-line hole array with the following parameters: MoGe film thickness: 50 nm; microbridge dimensions: 10 μm × 10 μm; nominal hole diameter: 200 nm; nominal lattice period: 400 nm. (b) $I_{c1}(H)$ (blue triangles) and $I_{c2}(H)$ (red open circles) dependences.

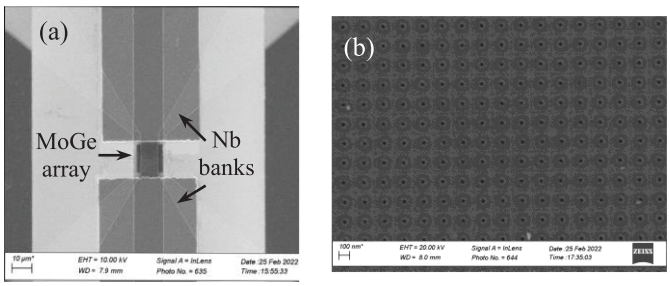

Fig. 6. (a) SEM picture of the array made on 50 nm thick MoGe microbridge with $w = 10$ μm. Array size is 15 μm × 10 μm; nominal hole diameter is 50 nm; lattice period is 180 nm. (b) Hole array on a magnified scale.

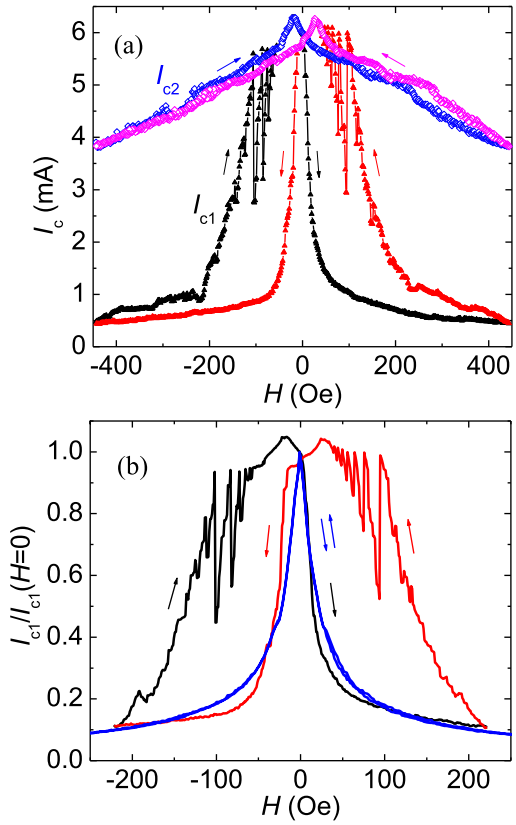

Fig. 7. (a) $I_{c1}(H)$ (solid triangles) and $I_{c2}(H)$ (open diamonds) patterns of the array taken in a relatively large interval of applied magnetic field. (b) I_{c1} vs H dependence of the same array measured in a smaller field range (black and red lines). I_{c1} is normalized to its maximum value at $H = 0$. For comparison, blue line shows $I_{c1}/I_{c1}(H = 0)$ vs H dependence of the unpatterned 10 μm × 10 μm microbridge. Arrows show the direction of field sweeping.

of unpatterned sample, but the $I_{c2}(H)$ pattern displays additional features compared with that for the unpatterned sample or the samples wherein the array is oriented perpendicular to the current flow. This is due to the fact that the in-line array is oriented perpendicular to the flux flow, and likely causes stronger vortex pinning than in the former case.

Next, we consider a square hole array made on a 50 nm thick MoGe microbridge with $w = 10$ μm; lateral dimensions of the array are 15 μm × 10 μm; nominal hole diameter is 50 nm; lattice period is 180 nm. In this sample, the array is situated between the 160 nm thick Nb banks deposited after the hole array is fabricated. The holes were made using e-beam lithography and ion milling.

Fig. 6(a) shows an SEM picture of the entire device including the microbridge with the array and Nb banks; Fig. 6(b) shows a portion of the array on a magnified scale. Fig. 7(a) shows $I_{c1}(H)$ (solid triangles) and $I_{c2}(H)$ (open diamonds) patterns of the array taken in a relatively large interval of applied magnetic field. Fig. 7(b) shows I_{c1} vs H dependence of the same array measured in a smaller field range (black and red lines). I_{c1} is normalized to its maximum value at $H = 0$. For comparison, blue line shows $I_{c1}/I_{c1}(H = 0)$ vs H dependence of the unpatterned 10 μm × 10 μm microbridge. Arrows show the direction of field sweeping.

Both $I_{c1}(H)$ and $I_{c2}(H)$ dependences are hysteretic; the interval of the currents where they coincide with each other is small. The hysteresis obviously occurs due to the presence of the hole array.

One can infer from Fig. 7(b) that the half width at half maximum (HWHM) of the $I_{c1}/I_{c1}(H = 0)$ dependence for an unpatterned 10 μm × 10 μm microbridge is almost the same as HWHM of the peak created by artificially combining the increasing field portions of the black and red branches for the array. In both cases there is drastic decrease of I_{c1} with H, which implies that flux entry at low field is almost insensitive to the presence of the holes. In turn, this implies that, in this regime, the penetration of vortices into the array occurs mainly through the interstitial region, since the area occupied by the holes is small compared to the total area.

Upon decreasing the field, there is an unusual feature in the $I_{c1}(H)$ pattern for the array (cf. Fig. 7): apart from an overall higher critical current relative to that for increasing fields, at lower fields, a series of sudden drops followed by subsequent buildups of I_{c1} is displayed. These features may be explained as follows. At high field, some vortices are pinned presumably to the holes. These vortices obstruct smooth escape of the flux that is not pinned, which results in rapid increase of the critical current when the field is swept down from higher levels. Due to the pinning force, the pinned vortices do not leave their sites on decreasing the field at low currents. When the field is further decreased and the current through the sample increases (to reach I_{c1} during its measurement), current-driven depinning of vortices occurs due to Lorentz forces. If some vortices escape from pinning centers, the energy dissipated by their motion will

Authorized licensed use limited to: Northwestern University. Downloaded on February 18,2024 at 00:22:00 UTC from IEEE Xplore. Restrictions apply.

favor further depinning, which may trigger vortex avalanches [10]. In this way, the pinned vortices are removed from the sample. Since, as we noted above, the process is dissipative, the critical current of the sample is temporarily reduced, leading to a dip in the $I_{c1}(H)$ pattern. The process can be repeated upon further field decreasing and current increasing, resulting in multiple dips and spikes.

We note that the fields at which spike-like structures emerge are considerably lower than that for the first commensurate field peak: i.e., the vortices are pinned at a density of less than one per hole. As is pointed out by Pla and Nori [11], at low pinning densities, the unpinned vortices can move a short distance before they are stopped by other pinned vortices. Such short vortex jumps may also lead to the I_{c1} drops and subsequent recovery of I_{c1} when the broken loose vortices are pinned again. The two processes – avalanches leading to escape of vortices from the sample, and sudden short vortex jumps – may coexist resulting in the observed I_{c1} jumps.

IV. Conclusion

We have fabricated and studied characteristics of unpatterned microbridges made of 50 nm thick MoGe films and hole arrays of different type made on nominally identical microbridges. The devices were characterized at 4–4.2 K. Two critical currents were measured as a function of an external perpendicular field applied: one that determines the transition into a resistive state, and a second, a flux-flow instability current, that determines the transition into a high-resistance state. Unusual non-monotonic dependence was observed for the second current in unpatterned and line-array microbridges resembling the modulation pattern in Josephson junctions. In the dense square lattice array of nanoholes, spike-like structures were observed in the dependence of the first critical current on applied magnetic field. The underlying physics of these behaviors deserves further study.

References

[1] V. V. Moshchalkov et al., "Quantum interference and confinement phenomena in mesoscopic superconducting systems," *Physica Scripta*, vol. 55, pp. 168–176, Mar. 1994, doi: 10.1088/0031-8949/1994/T55/030.

[2] G. Blatter et al., "Vortices in high-temperature superconductors," *Rev. Modern Phys.*, vol. 66, no. 4, pp. 1125–1388, Oct. 1994, doi: 10.1103/RevModPhys.66.1125.

[3] E. H. Brandt, "The flux-line-lattice in superconductors," *Rep. Prog. Phys.*, vol. 58, no. 11, pp. 1465–1594, Nov. 1995, doi: 10.1088/0034-4885/58/11/003.

[4] J. M. Graybeal and M. R. Beasley, "Observation of a new universal resistive behavior of two-dimensional superconductors in a magnetic field," *Phys. Rev. Lett.*, vol. 56, no. 2, pp. 173–176, Jan. 1986, doi: 10.1103/PhysRevLett.56.173.

[5] M. Liang, M. Kunchur, J. Hua, and Z. Xiao, "Evaluating free flux flow in low-pinning molybdenum-germanium superconducting films," *Phys. Rev. B*, vol. 82, Aug. 2010, Art. no. 064502, doi: 10.1103/PhysRevB.82.064502.

[6] I. Roy et al., "Melting of the vortex lattice through intermediate hexatic fluid in an a-MoGe thin film," *Phys. Rev. Lett.*, vol. 122, no. 4, Jan. 2019, Art. no. 047001, doi: 10.1103/PhysRevLett.122.047001.

[7] J. Pearl, "Current distribution in superconducting films carrying quantized fluxons," *Appl. Phys. Lett.*, vol. 5, no. 4, pp. 65–66, Aug. 1964, doi: 10.1063/1.1754056.

[8] I. P. Nevirkovets, M. A. Belogolovskii, and J. B. Ketterson, "Josephson junctions based on amorphous MoGe: Prospects for use in superconducting electronics," *Supercond. Sci. Technol.*, vol. 35, no. 3, Mar. 2022, Art. no. 035008, doi: 10.1088/1361-6668/ac4b00.

[9] G. Grimaldi et al., "Speed limit to the Abrikosov lattice in mesoscopic superconductors," *Phys. Rev. B*, vol. 92, no. 2, Jul. 2015, Art. no. 024513, doi: 10.1103/PhysRevB.92.024513.

[10] J. I. Vestgården, D. V. Shantsev, Y. M. Galperin, and T. H. Johansen, "Lightning in superconductors," *Sci. Rep.*, vol. 2, Nov. 2012, Art. no. 886, doi: 10.1038/srep00886.

[11] O. Pla and F. Nori, "Self-organized critical behavior in pinned flux lattices," *Phys. Rev. Lett.*, vol. 67, no. 7, pp. 919–922, Aug. 1991, doi: 10.1103/PhysRevLett.67.919.

Authorized licensed use limited to: Northwestern University. Downloaded on February 18,2024 at 00:22:00 UTC from IEEE Xplore. Restrictions apply.